

# EFFECT OF ROUGHNESS ON THE SPATIO-TEMPORAL CHARACTERISTICS OF INNER-OUTER INTERACTIONS IN A TURBULENT BOUNDARY LAYER

**Gokul Pathikonda**

Department of Aerospace and Mechanical Engineering  
University of Notre Dame, Notre Dame  
Currently at: Department of Mechanical Engineering  
Georgia Institute of Technology, Atlanta

**Kenneth T. Christensen**

Departments of Aerospace & Mechanical Engineering and  
Civil & Environmental Engineering & Earth Sciences  
University of Notre Dame, Notre Dame

## ABSTRACT

Turbulent boundary layers over smooth and rough walls are investigated using high frame-rate PIV in a refractive-index-matched (RIM) flow facility to better understand the structure of inner-outer modulating interactions. The RIM enables well resolved investigation of the near-wall buffer and roughness sub-layers to identify the effect of large and very large scales on the same. A hexagonally-packed hemispherical roughness pattern is investigated, together with baseline measurements over a smooth wall. Amplitude and frequency modulation coefficients are computed for each case, and preliminary results have shown strong correlation coefficients over roughness compared to the smooth-wall baseline. The wall-normal velocity fluctuations in the roughness sub-layer are stronger compared to that in the smooth-wall near-wall region, and exhibit frequency modulation. The on-going work aims to investigate the effect of roughness geometry on this interaction structure using conditional averaging methods.

## INTRODUCTION

The exploration of the modulations of near-wall turbulence by the very large-scale structures in wall-bounded turbulent flows has garnered significant interest in recent years. With increasing  $Re$  in these flows, the large- and very large-scale motions become increasingly stronger, while simultaneously developing (by definition a high  $Re$ ) a large temporal and spatial scale separation between them and the near-wall smaller scales. This was shown to yield amplitude and frequency (and possibly scale) modulations of the latter by the former (Mathis *et al.*, 2009; Ganapathisubramani *et al.*, 2012). This amplitude modulation (AM) was also observed on wall skin friction traces (Mathis *et al.*, 2013), indicating the practical significance of these interactions. These modulation interactions highlight the presence of turbulent phenomena that are dominant only at higher  $Re$ , and that must be understood to develop effective models for use in

real world applications.

Many recent works have extended the initial works of Mathis *et al.* (2009) in identifying similar phenomena in other kinds of turbulent flows such as jets, flows with discrete roughness elements, rough-wall flows, etc. Theoretical frameworks that attempt to explain these interactions were proposed based on the quasi-steady, quasi homogeneous (QSQH) hypothesis, resolvent modes, attached eddy hypothesis, etc. Models to accommodate AM based on simple superposition (Mathis *et al.*, 2011) and linear stochastic estimation have been proposed, and used for LES simulations to model unresolved SGS scales. Recent works based on hot-wire measurements and applying Taylor's hypothesis (Baars *et al.*, 2015) have proposed a mean spatial structure for these inner-outer interactions. The current work is a part of this recent interest to observe, define and better understand this phenomena so as to lead to improved predictive capabilities of flows involving high  $Re$  turbulent boundary layers. By using refractive-index matching (RIM) and highly-resolved PIV measurements, we aim to better understand the spatio-temporal structure of inner-outer interactions. In particular, we aim to understand the effects of the wall roughness and its geometry on the nature of these interactions as well as to extend our recent observations for flow over smooth walls (Pathikonda & Christensen, 2019) to a rough-wall boundary layer, to eventually aid development of LES models for high  $Re$  simulations of flow over realistic rough walls (Pathikonda & Christensen, 2017).

## EXPERIMENTS

All experiments were performed in the small RIM flow facility at the University of Notre Dame – a closed loop liquid facility. The test section is 2.5 m long from entry to exit, has a square cross-section of side length 112 mm. The working solution for the facility is a saturated solution of sodium iodide (NaI), with a refractive index of  $RI = 1.491$ , which is matched to that of the acrylic test section and floor.

Matching the RI of the working solution with that of the test section floor avoids strong near-wall reflections of the laser sheet which typically plague PIV measurements of flow over rough walls in wall-normal planes. This thus enables accurate interrogation of the velocity within the buffer and roughness sub-layers (in smooth- and rough-wall flow, respectively), without being hindered by wall reflections. This is particularly crucial to the current work, since much of the modulated small scales reside in the immediate vicinity of the wall ( $y^+ < 30 - 50$ ).

Two sets of experiments with different wall conditions were performed under near-identical conditions – smooth-wall (SW) and hemispherical rough-wall (HS-RW) boundaries. While the boundary layer on the floor of the test section was used for the smooth-wall measurements, cast roughness panels were mounted on this floor for the rough-wall measurements. Hexagonally-packed hemispherical roughness (2 mm dia.) was produced for the latter, where uniform mating roughness panels were cast using urethane with an RI close to that of the working fluid. A detailed spatio-temporal analysis of the current smooth-wall data, including details of the experimental setup, was presented in Pathikonda & Christensen (2019) and is included herein as a baseline case. The same experimental approach was utilized for the rough-wall case, so further details on the experimental setup, and the considerations for PIV measurements to investigate modulating interactions, can be found in this reference.

The PIV system consists of two high-frame-rate, 4 MP Phantom V641 cameras, that are capable of measuring 700 vector fields per second at full resolution. Two cameras (simultaneously measuring a big field of view (bFOV) and a small one (sFOV)) were placed on opposite sides of a streamwise-wall-normal-oriented light sheet. The bFOV had a large FOV that captured velocity structures over a larger streamwise extent ( $2\delta$ , where  $\delta$  is the boundary layer thickness) at lower spatial resolution. The sFOV has a smaller FOV ( $0.7\delta$ ) that specifically resolved the smaller scales near the wall. A high-repetition, dual cavity, Northrop Grumman Patara laser capable of up to 54 mJ/pulse at 1000 Hz was used for illumination, and the entire PIV system was run synchronously at  $F_s = 700$  Hz ( $F_s y^*/u_\tau \sim 3$ ). The flow was seeded with 2-micron tracer particles at a high seeding density to ensure high spatial resolution in the sFOV. Table 1 lists various boundary-layer parameters and details of these experiments.

Table 1. Measurement and flow parameters of experiments.

Label	SW	RW
Vector fields per second	700 Hz	700 Hz
No. datasets	20	20
Vector fields per dataset	2734	2734
Free-stream velocity ( $U_\infty$ , m/s)	1.07	1.07
Boundary layer height ( $\delta$ , mm)	38	34
Kármán number ( $Re_\tau$ )	1410	1350
Skin-friction velocity ( $u_\tau$ , m/s)	0.045	0.048
Viscous length scale ( $y^*$ , $\mu\text{m}$ )	27	25.4

## MEAN BOUNDARY-LAYER CHARACTERISTICS

Time-uncorrelated ensembles of 2000 vector fields acquired at 20 fields-per-second in both smooth- and rough-wall flow were first captured over a FOV that extended beyond the edge of the boundary layers to compute single-point statistics, mean boundary-layer parameters and velocity spectra. A non-linear regression fit of the mean velocity profile was performed to the theoretical form proposed by Chauhan *et al.* (2007). A parameter space of ‘true’ boundary layer ( $\tilde{\delta}$ ), virtual origin correction ( $y_c$ ), friction velocity ( $u_\tau$ ), wake parameter ( $\Pi$ ) and the velocity defect due to wall roughness  $\Delta U$  were determined in this regard. Following the modified Clauser chart method (Perry & Li, 1990) and to exclude the effects of the roughness sub-layer, this fit was performed only to points above the momentum thickness,  $\theta$ . A unique, converged parameter set was obtained with the virtual origin below the tip of the hemispherical roughness, and was found to be reasonably insensitive to the initial guesses of the parameter space.

Figure 1a-c presents the variation of mean velocity ( $U^+$ ), streamwise Reynolds normal stress ( $\overline{u^{+2}}$ ) and skewness of the streamwise velocity fluctuations ( $u_{sk} = \overline{u^{+3}} / (\overline{u^{+2}})^{3/2}$ ) for the rough-wall case, together with that from the baseline smooth-wall case. The rough-wall boundary layer shows a wake profile more representative of a canonical boundary layer than the smooth-wall case. We suspect this to be due to a slight favorable gradient in the latter case, and possibly due to the trip mechanism. The observations of the current work, however, are not affected by this change as they are related to the flow dynamics very close to the wall. Additionally, the profiles of  $\overline{u^{+2}}$  and  $u_{sk}$  show the effect of roughness in altering the near-wall turbulence, where the inner peak of the former and representative of turbulence production is weaker.

The spatial information available from the current PIV data enables one to compute the spatial spectrum of the streamwise and wall-normal velocity fluctuations. Figure 1(d,e) shows the distribution of the streamwise and wall-normal TKE contributions at various wavelengths computed from the bFOV data. The roughness sub-layer embodies structures  $\lambda_x^+ \gtrsim 1000$ , the strength of which is less than that of the baseline smooth-wall case (Pathikonda, 2017, *not shown here*). This similarity of the small-scale dynamics near the wall can be attributed to the low equivalent sandgrain roughness height ( $k_s^+ = 16$ ) of the roughness and the boundary layer. The wall-normal velocity fluctuations in the logarithmic region, however, are stronger in the rough-wall case compared to that of the smooth-wall flow (Pathikonda, 2017, *not shown here*). The temporal spectra form the high-speed data has also been computed, and was found to be identical to the spatial spectra in figure 1(d,e). With this understanding of the mean and spectral characteristics of the boundary layer, inner-outer modulation effects can be investigated. For the current work, we make use of the measurements to perform a ‘temporal-only’ analysis, where only the temporal evolution of velocity fluctuations across the boundary layer akin to that performed conventionally using hot-wire anemometry.

## AMPLITUDE MODULATION

The amplitude modulation (AM) of the near-wall streamwise velocity fluctuations was characterized using Hilbert transforms by Mathis *et al.* (2009), and Mathis

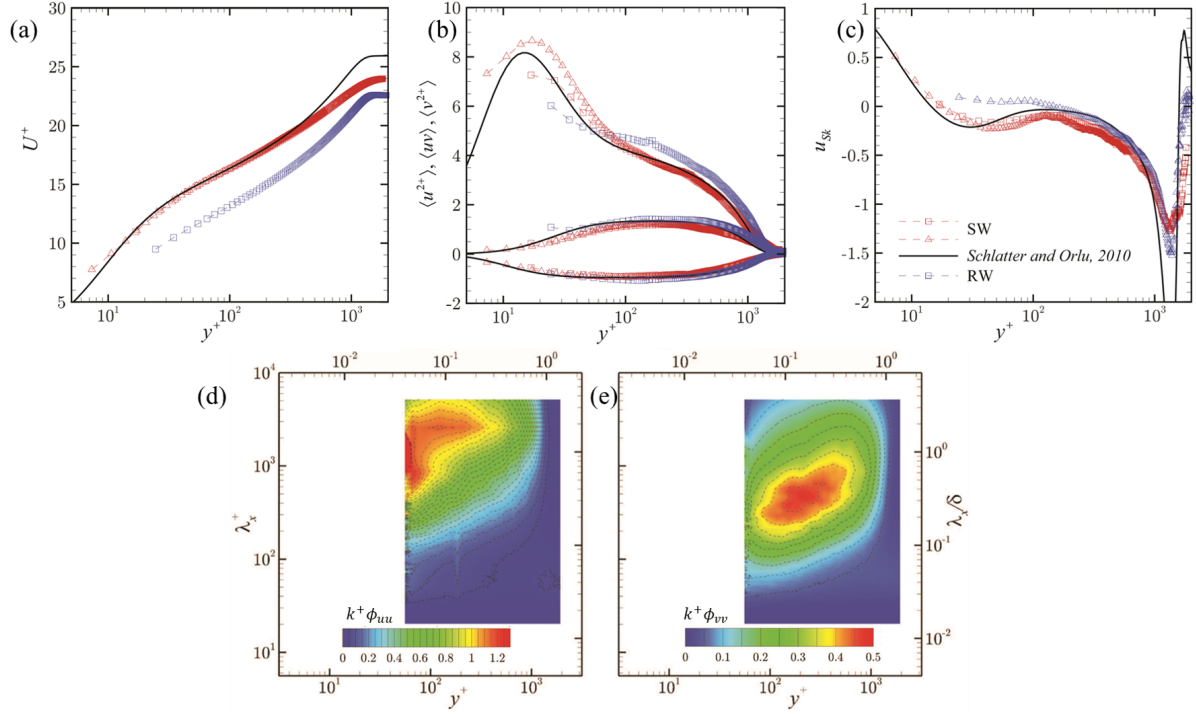


Figure 1. Wall-normal profiles of (a) mean streamwise velocity, (b) in-plane Reynolds stresses, and (c) skewness of streamwise velocity fluctuations from measured smooth-wall and rough-wall cases and from the computations of Schlatter & Örlü (2010). Also shown are the spatial spectra of (d) streamwise and (e) wall-normal velocity fluctuations from the bFOV for the rough-wall case (see Pathikonda, 2017, for SW).

*et al.* (2011) soon extended the observations for a predictive model of the same. Besides Hilbert transforms, AM has also been investigated using small-scale integrals of wavelet power spectra (Baars *et al.*, 2015), small-scale variance (Ganapathisubramani *et al.*, 2012, etc.), for flow over rough walls (Squire *et al.*, 2016; Pathikonda & Christensen, 2017; Basley *et al.*, 2018; Awasthi & Anderson, 2018), channel and pipe flows (Wu *et al.*, 2019), and other complex flows. For the current work, we utilize the method of Hilbert transform to study the AM correlation coefficient,  $R^a$ , of the near-wall small scales by the outer large scales. This correlation is obtained by correlating the large-scale envelope of the small scales with the large scales sampled either locally ('1-point') or within the logarithmic region ('2-point'). Further details on this method can be found in the original work of Mathis *et al.* (2009). Figure 2(a,b) shows the AM correlation coefficients computed for flow over the hemispherical roughness, using the '1-point' ( $R_a^{1P}$ ) and the '2-point' ( $R_a^{2P}$ ) techniques. For the former, the large scales are sampled locally with the small scales and the correlation coefficient is computed (as  $R_a^{1P}$ ). For the latter, the small scales are sampled at various wall-normal positions (similar to  $R_a^{1P}$ ), whereas the large scales are always sampled at a fixed position centered in the logarithmic region ( $y_o = \sqrt{15Re_\tau}$ ). The latter approach is a more direct measure of AM, since the true outer signature of the large scales is sampled independent of the location of the small scales, which is particularly important in rough-wall flows where the superposition of the large scales on near-wall velocity fluctuations can be limited by roughness effects. Both  $R_a^{1P}$  and  $R_a^{2P}$  show a sharp increase in the near-wall region, similar to their smooth-wall counterparts, with the later being consistently higher than the former and both correlations being higher in the rough-wall case than that of the smooth-

wall flow. These observations are entirely consistent with previous findings in rough-wall flow where a higher correlation was observed over roughness compared to a smooth wall (Squire *et al.*, 2016; Pathikonda & Christensen, 2017).

The availability of temporally-resolved fluctuations across the the boundary layer enabled computation of multi-point correlation maps, as was demonstrated by Bernardini & Pirozzoli (2011) from DNS data. These correlation maps for the streamwise and wall-normal velocity fluctuations are shown in figure 2(c,d), where the horizontal and vertical axes demarcate the locations where the large and small scales were sampled ( $y_o$  and  $y_i$ , respectively). Extracting the correlations along the diagonal  $y_o = y_i$  recovers the '1-point' correlations shown in figure 2(a), while extracting that along  $y_o = \sqrt{15Re_\tau}$  recovers the 2-point correlations. The appearance of a strong outer peak at  $y_o \approx 100y^*$  demonstrates the enhanced AM in the rough-wall flow.

## FREQUENCY MODULATION

In addition to AM, the near-wall small scales have been previously found to be frequency modulated (FM) as well. Baars *et al.* (2015) used the wavelet power spectra, while Ganapathisubramani *et al.* (2012) used peak-counting of conditionally-sampled small scales to investigate this phenomena in smooth-wall flow. Pathikonda & Christensen (2017) and Awasthi & Anderson (2018) have subsequently investigated the same for flow over rough walls and observed that FM can be a more robust metric of inner-outer interactions compared to AM, especially for rough-wall boundary layers where the extent of the roughness sub-layer could overlap with the dynamics of the logarithmic region. To investigate FM correlation coefficients for the current rough-wall flow, a representative time series of small-scale

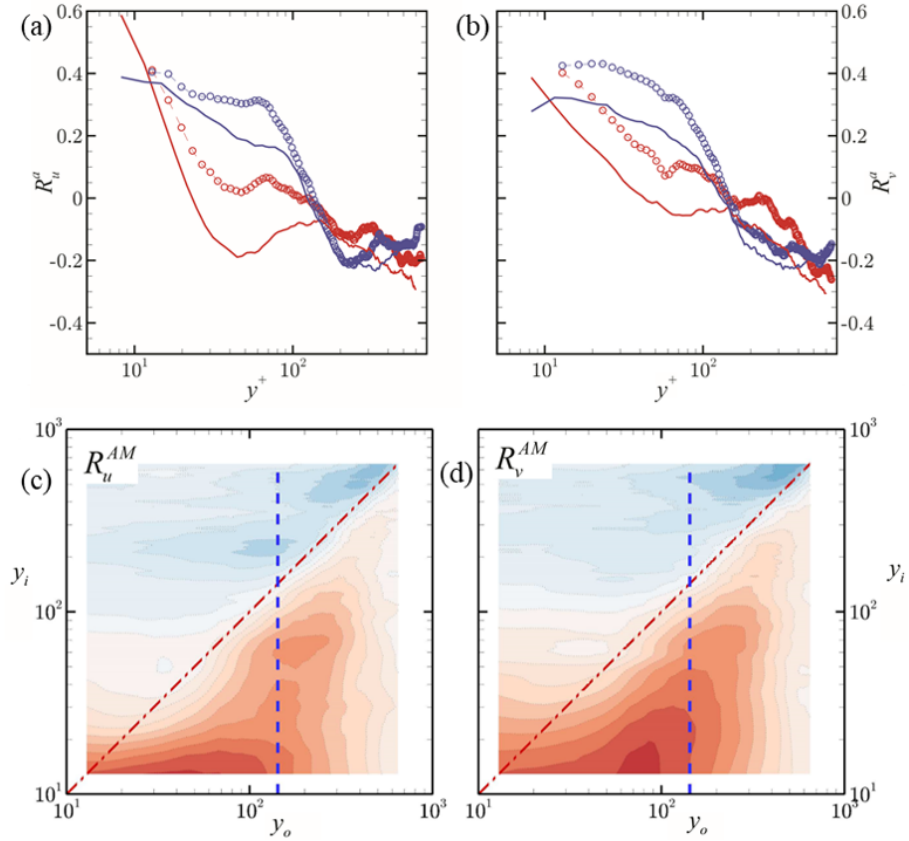


Figure 2. The wall-normal variation of amplitude modulation correlation coefficients of (a) streamwise and (b) wall-normal fluctuations. (c,d) The multi-point correlation map of the corresponding analysis for rough-wall (see Pathikonda & Christensen, 2019, for SW). *Solid lines* in (a,b) represent smooth-wall and symbols represent the rough-wall counterparts from *1-point (red)* and *2-point (blue)* analysis.

frequency is obtained using the continuous wavelet transform of the velocity fluctuations, which is then correlated with the large scales. More detailed explanation of this method of analysis can be found in the original work of Baars *et al.* (2015). Similar to the AM counterparts, the ‘*1-point*’ and ‘*2-point*’ FM correlation coefficients were computed based on the location where the large scales are sampled.

Figure 3(a,b) shows the FM correlation coefficients corresponding to streamwise and wall-normal velocity fluctuations, compared with their smooth-wall counterparts. Albeit weaker than AM, the rough-wall flow exhibits clear FM of near-wall small scales by both local and log-region large scale fluctuations.  $R_u^{FM}$  shows similar trends in wall-normal variation, albeit stronger than the smooth-wall baseline. A distinction between the two cases is observed in the near-wall behavior of  $R_v^{FM}$ . While the coefficients anomalously tend towards zero in the smooth-wall case, the same behavior is not observed in the rough-wall flow as they tend to plateau to a non-zero value. This difference could be due to a strong suppression of the wall-normal velocity fluctuations in flow over smooth walls compared to the rough-wall case. This, coupled with the finite resolution effects of PIV in measuring wall-normal fluctuations and a sensitivity of FM coefficients to noise, could be leading to this behavior over smooth walls as has previously been discussed in Pathikonda & Christensen (2019). The current observations in rough-wall flow support this suspicion of the anomaly, which show stronger wall-normal velocity fluctuations as was also seen in figure 1. Finally, similar to AM, 2-D FM

correlation maps were constructed based on the availability of simultaneous velocity fluctuations across the boundary layer. Figure 3(c,d) shows a FM-structure similar to that of figure 2 for AM, in both the  $u$ - and  $v$ - correlation maps. The presence of an outer peak near the wall at  $y_o \approx 100y^*$  demonstrates the enhanced FM in rough-wall flow.

## CONCLUSIONS AND FUTURE WORK

The current work investigates amplitude and frequency modulation effects via high-frame-rate, dual field-of-view PIV measurements in a refractive-index-matched flow facility. This is an extension of a similar analysis conducted for smooth-wall flow reported in Pathikonda & Christensen (2019) which provides a spatio-temporal picture of these interactions using conditional averaging techniques. The current work measures the mean structure of the boundary layer over hexagonally-packed hemispherical roughness and, using temporal analysis, reports the *1-*, *2-* and multi-point correlation coefficients for amplitude and frequency modulation embodied in streamwise and wall-normal velocity fluctuations. We observe similar characteristics of stronger AM correlation coefficients in rough-wall flow (compared to smooth-wall flow), and finite FM coefficients. An anomalous decrease in near-wall  $R_v^{FM}$  in smooth-wall flow was found to be absent in the rough-wall results, supporting the hypothesis that this could be from a more stringent no-penetration condition imposed by the smooth wall.

The current work leveraged the availability of velocity data across the boundary layer as a series of temporally-

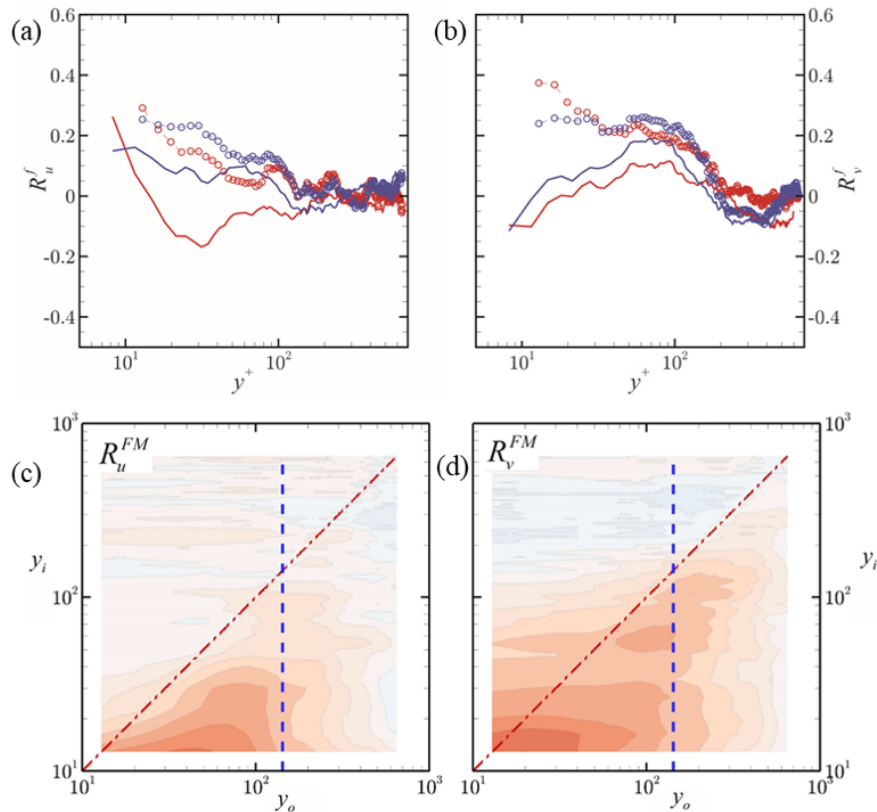


Figure 3. As in figure 2, but for frequency modulation.

resolved point measurements to show AM and FM correlations as traditionally computed from hot-wire anemometry measurements. With this preliminary demonstration of the ability to capture AM and FM effects using high-frame-rate PIV, the ongoing efforts include exploring the spatio-temporal structure based on conditional averages in rough-wall flow, similar that reported for smooth-wall flow in Pathikonda & Christensen (2019). The near-wall structure over the hemispherical roughness is expected to be markedly different than that of the smooth-wall flow and a spatial analysis will provide additional details on the mechanisms of these inner-outer interactions in the presence of roughness.

## REFERENCES

- Awasthi, A. & Anderson, W. 2018 Numerical study of turbulent channel flow perturbed by spanwise topographic heterogeneity: Amplitude and frequency modulation within low-and high-momentum pathways. *Physical Review Fluids* **3** (4), 044602.
- Baars, W. J., Talluru, K. M., Hutchins, N. & Marusic, I. 2015 Wavelet analysis of wall turbulence to study large-scale modulation of small scales. *Exp. Fluids* **56** (10), 1–15.
- Basley, J., Perret, L. & Mathis, R. 2018 Spatial modulations of kinetic energy in the roughness sublayer. *Journal of Fluid Mechanics* **850**, 584–610.
- Bernardini, M. & Pirozzoli, S. 2011 Inner/outer layer interactions in turbulent boundary layers: a refined measure for the large-scale amplitude modulation mechanism. *Phys. Fluids* **23** (6), 061701.
- Chauhan, K., Nagib, H. M. & Monkewitz, P. A. 2007 On the composite logarithmic profile in zero pressure gradient turbulent boundary layers. In *Proc. 45th AIAA Aerospace Sciences Meeting, Paper No. AIAA*, vol. 532, pp. 1–18.
- Ganapathisubramani, B., Hutchins, N., Monty, J. P., Chung, D. & Marusic, I. 2012 Amplitude and frequency modulation in wall turbulence. *J. Fluid Mech.* **712**, 61–91.
- Mathis, R., Hutchins, N. & Marusic, I. 2009 Large-scale amplitude modulation of the small-scale structures in turbulent boundary layers. *J. Fluid Mech.* **628**, 311–337.
- Mathis, R., Hutchins, N. & Marusic, I. 2011 A predictive inner–outer model for streamwise turbulence statistics in wall-bounded flows. *J. Fluid Mech.* **681**, 537–566.
- Mathis, R., Marusic, I., Chernyshenko, S. I. & Hutchins, N. 2013 Estimating wall-shear-stress fluctuations given an outer region input. *Journal of Fluid Mechanics* **715**, 163–180.
- Pathikonda, Gokul 2017 Inner-outer interactions in a rough-wall turbulent boundary layer. PhD thesis, University of Illinois at Urbana-Champaign.
- Pathikonda, Gokul & Christensen, K. T. 2017 Inner–outer interactions in a turbulent boundary layer overlying complex roughness. *Phys. Rev. Fluids* **2** (4), 044603.
- Pathikonda, G. & Christensen, K. T. 2019 Investigation of inner-outer interactions in a turbulent boundary layer using high-speed particle image velocimetry. *Physical Review Fluids* **4** (3), 034607.
- Perry, A. E. & Li, D. J. 1990 Experimental support for the attached-eddy hypothesis in zero-pressure-gradient turbulent boundary layers. *Journal of Fluid Mechanics* **218**, 405–438.
- Schlatter, P. & Örlü, R. 2010 Assessment of direct numerical simulation data of turbulent boundary layers. *Journal of Fluid Mechanics* **659**, 116.
- Squire, D. T., Baars, W. J., Hutchins, N. & Marusic, I. 2016 Inner–outer interactions in rough-wall turbulence. *Jour-*

*Journal of Turbulence* **17** (12), 1159–1178.  
Wu, Sicong, Christensen, Kenneth T & Pantano, Carlos  
2019 Modelling smooth-and transitionally rough-wall

turbulent channel flow by leveraging inner–outer interactions and principal component analysis. *Journal of Fluid Mechanics* **863**, 407–453.